Cerium doped copper/ZSM-5 catalysts used for the selective catalytic reduction of nitrogen oxide with ammonia

Baojuan Dou[a], Gang Lv[b] , Chang Wang [a], Qinglan Hao[a,*], KwanSan Hui[c, **]

[a] *College of Marine Science & Engineering, Tianjin University of Science & Technology, 13 St. TEDA, Tianjin, 300457,PR China*

[b] *State Key Laboratory of Engines, Tianjin University, Weijin Road 92, Tianjin 300072, PR China*

[c]*Department of Mechanical Convergence Engineering, Hanyang University, 17 Haen gdang-dong, Seongdong-gu, Seoul 133-791, Republic of Korea*

Abstract:

The CuCe/ZSM-5 catalysts with different cerium loadings (0, 0.5, 1.0, 1.5 and 2.0 wt.%) was investigated to evaluate the correlation between structural characteristics and catalytic performance for the selective catalytic reduction (SCR) of NO by NH_3. It was found that the addition of cerium increased copper dispersion and prevented its crystallization. According to the results of X-ray photoelectron spectroscopy (XPS) and temperature-programmed reduction by hydrogen (H_2-TPR), copper species were enriched on the ZSM-5 grain surfaces and part of copper ions was incorporated into the cerium lattice. Addition of cerium improved the redox properties of the CuCe/ZSM-5 catalysts, owing to the higher valence of copper and mobility of lattice oxygen than those of Cu/ZSM-5 catalyst. Hence the introduction of

* Corresponding author. Tel.: +86-22-60601278; Fax.: +86-22-60600320
E-mail address: haoqinglan@tust.edu.cn
** Corresponding author. Tel.: +822 2220 0441; fax: +822 2220 2299 (K. Hui)E -mail address: kshui@hanyang.ac.kr (K. Hui)

cerium in Cu/ZSM-5 improved significantly NO conversion. On the one hand, the cerium introduction into Cu-Z enhances their low-temperature activities. 95% NO conversion is reached around 197 ºC for Cu-Z while the corresponding temperature value decreases to 148 ºC for CuCe4-Z. On the other hand, the temperature range of efficient NO reduction (95%) also extends to higher temperature when the cerium are added to Cu/ZSM-5. Among the Cu-Ce/ZSM-5 catalysts tested, the CuCe4-Z sample exhibits the highest catalytic activity with the temperature range for 90% NO removal of 148-427 ºC.

Keywords: Selective catalytic reduction; CuCe/ZSM-5 catalyst; Nitrogen oxide; Ammonia

Introduction

Nitrogen oxides (NO_x) are hazardous to human health, contributing to seriously environmental problems. Selective catalytic reduction (SCR) of NO_x by NH_3 is an efficient technology for controlling NO_x emissions [1]. Ever since Iwamoto et al [2] reported that the Cu-ZSM-5 catalyst showed high activity of selective catalytic reduction of NO_x, much work has been performed to explore the catalytic properties of those catalysts, especially for on-road applications [3,4]. The utility of ZSM-5 as catalyst supports derives significantly from their remarkable ion-exchange capacity [5]. For the reaction mechanism over copper exchanged zeolites, different copper species which is active for SCR reaction were identified in Cu/ZSM-5, mainly including isolated ions either in framework positions or in cationic positions in the

zeolite channels, copper clusters in extra-framework positions, copper oxide located at the surface of the zeolite crystal [6,7]. When the temperature increases, these copper species exhibit the catalytic activity with turnover frequency decreasing in the order: isolated copper ions > copper clusters > copper oxide. Hence the Cu/ZSM-5 exhibits a wider operation window than commercial V_2O_5-WO_3/TiO_2 catalysts.

It is well known that the key factors determining the activity and selectivity of supported catalysts are the nature and dispersion of copper species, which depend approximately on the aluminum content in the framework and the copper loading ratio [8,9]. Many researches demonstrated that the most active catalysts tend to have the lowest Si/Al atomic ratio because only copper ions close to framework AlO_4^- are active in the decomposition of NO into N_2 [10-12]. Unfortunately, too much aluminum anchored in the framework of ZSM-5 led to marked decrease in hydrothermal stability. The catalytic activity of Cu/ZSM-5 increases with enhancing copper content, reaching a maximum of NO_x conversion, and then decreases at higher contents. The reason for activity saturation is attributed to the grains of copper oxides growing up at high copper content because they promote inevitably the reductant oxidation in the presence of oxygen [13,14]. Considering the exhaust temperatures of automotives often varying in a wide range from 150 °C during a cold start to 600 °C for top-load operation, the existing active window of existing Cu/ZSM-5 is still unable to meet the requirement of various running mode of diesel engines.

To further enlarge the temperature window of application, a second metal is often introduced into Cu/ZSM-5 as additives. The combination and interaction between two

metal elements significantly influence its bulk and surface physiochemical structure [15,16]. Ceria has been employed as a promoter for metal-containing ZSM-5 catalysts and its wide application is attributed to some special properties, such as: (1) the redox couple between the trivalent and tetravalent oxidation states of the ceria ions that allow easy oxygen exchange with the medium; (2) formation of labile oxygen vacancies and oxide ion storage; (3) to increase the dispersion and stability of the active form of the metal by strong metal-support interaction [17,18]. Sowade et al. [19] believed that In/ZSM-5 catalysts for the SCR of NO by methane are effectively promoted by extra-zeolite CeO_2. The CeO_2 is beneficial to catalyzing NO oxidation to provide a rich NO supply and acts independently from the other catalyst components. Similarly, Qi et al. [20] confirmed that ceria could promote the oxidization of NO to NO_2, thus increasing the catalyst activity for SCR of NO with NH_3. Carja et al. [21] synthesized MnCe/ZSM-5 catalyst by an aqueous phase method which exhibited a broad temperature window (244-550 °C) for high NO conversions (75-100%) even in the presence of H_2O and SO_2.

Herein, more attentions were focused on CuO_x-CeO_2 since its favorable properties in catalytic oxidation reactions, such as diesel soot, [22] volatile organic compounds [23] and carbon monoxide [24] etc. The reaction path follows a rodox mechanism, involving the change of the oxidation state of both copper ($Cu^{2+}\leftrightarrow Cu^{+}$) and cerium ($Ce^{4+}\leftrightarrow Ce^{3+}$). Up to data, however, few works are reported in the literature to evaluate SCR using Cu-Ce based zeolites. The present study focused on the effects of ceria addition on the structures and copper species in copper-based

ZSM-5 catalysts. The catalytic behavior of obtained materials was tested in selective catalytic reduction of NO_x using ammonia as reductant. The characterizations of the catalysts were analyzed through several characterization techniques, such as nitrogen sorption, X-ray powder diffractometer (XRD), scanning electron microscopy (SEM), and transmission electron microscopy (TEM), X-ray photoelectron spectroscopy (XPS), temperature-programmed desorption of NH_3 measurement (NH_3-TPD) and temperature-programmed reduction by hydrogen (H_2-TPR).

2. Experimental

2.1. Catalyst preparation

H/ZSM-5 with an atomic Si/Al ratio of 25 and crystallinity of 100% was supplied by Nankai University, Tianjin, P. R. China. The Cu/ZSM-5 and CuCe/ZSM-5 catalysts were prepared by a conventional ion-exchange technique [25]. An appropriate amount of copper and ceria nitrate were dissolved in deionized water and mixed with 0.5 g of H/ZSM-5. The resulting solution was stirred at 80 °C for 24 h, at a pH of about 7.0. After being filtered and dried by evaporation, the sample was calcined in air at 600 °C for 4 h. The copper and cerium concentrations of each calcined catalyst were determined by using a PerkinElmer AAnalyst 300 Atomic Absorption spectrometer (AAS). To evaluate the influence of cerium content on the Cu/ZSM-5 property of selective catalytic reduction of NO_x, the copper content of the catalyst is set at 2.0 wt.%, and the cerium contents are 0, 0.5, 1.0, 1.5 and 2.0 wt.%, corresponding to Cu-Z, CuCe1-Z, CuCe2-Z, CuCe3-Z and CuCe4-Z, respectively.

2.2. Characterization

Nitrogen adsorption was measured with a NOVA 2000 gas sorption analyzer at liquid nitrogen temperature (-196 °C). Prior to measurement, each sample was degassed under vacuum for 8 h at 300 °C. The Brunauer-Emmett-Teller (BET) method was utilized to calculate the specific surface area using adsorption data acquired at a relative pressure (P/P_0) range of 0.05-0.25. The total pore volume was estimated from the amount of nitrogen adsorbed at a relative pressure of about 0.99. Pore size distribution curves were calculated using the Howarth-Kawazoe (HK) formalism for micropores and the Barret-Joyner-Halenda (BJH) method from the adsorption branch for mesopores. The crystalline phase was determined by powder XRD using a Rigaku D/MAC/max 2500v/pc instrument with Cu Kα radiation (40 kV, 200 mA, λ=1.5418 Å). Diffractometer data were acquired with a step size of 0.02° for 2θ values from 5-60°. TEM images of catalysts were observed with a Philips Tecnai G^2 F20 microscope operating at 200 kV coupled with an Oxford-1NCA EDX detector. Prior to TEM analysis, samples were dispersed in ethanol by sonication and deposited on a copper grid coated with a carbon film. XPS spectra were recorded on a Perkin-Elmer PHI-1600 ESCA spectrometer using Mg Kα X-ray source. The binding energies were calibrated using C1s peak of contaminant carbon (BE = 284.6 eV) as an internal standard. Temperature-programmed desorption of ammonia measurement (NH_3-TPD) test was performed in a Micromeritics Autochem 2920 II analyzer with the thermal conductivity detector (TCD). After being pretreated at 300 °C under flowing helium (50 mL min^{-1}) for 1 h, the powder sample (100 mg) was cooled to

50 °C, and then adsorbed to saturation by pulses of ammonia for 0.5 h. Physically adsorbed ammonia on catalyst was removed by flushing the sample with helium (50 mL min^{-1}) for 1 h at the adsorption temperature. Thermal desorption of ammonia was carried out in the temperature range of 50-600 °C at an increasing temperature rate of 10 °C min^{-1}. Temperature-programmed reductions with hydrogen (H_2-TPR) experiments were also performed with a Micromeritics Autochem 2920 II analyzer equipped with TCD. For the analysis, 100 mg of sample was pre-treated in 20% oxygen at 600 °C for 30 min. After cooling to 50 °C, the H_2-TPR was recorded in 10 vol.% H_2, with a heating rate of 10 °C min^{-1} and a final temperature of 600 °C.

2.3. Catalytic activity testing

Catalytic experiments were performed at atmospheric pressure in a flow-type apparatus designed for continuous operation. Before each test run, the catalyst powder was first pressed into a wafer and sieved into 20-40 meshes, and then 0.5 g of the catalyst was packed into a fixed-bed reactor made of a quartz tube with an internal diameter of 10 mm. A K-type thermocouple was located inside the catalyst bed to monitor reaction temperature. The reaction was carried out across the temperature range 30-300 °C, and the feed gas (1000 ppm NO, 1000 ppm NH_3, 10% O_2 and N_2 to balance; space velocity (SV) of 15,000 h^{-1}) was metered using calibrated electronic mass flow controllers. The concentration of NO, NO_2, N_2O and NH_3 were monitored by using the on-line quadrupole mass spectrometer (OmniStar 200).

3. Results and discussion

3.1. Structure and morphology

Fig. 1 shows the nitrogen adsorption-desorption isotherms for pure ZSM-5 and CuCe/ZSM-5 catalysts. According to the IUPAC classification, the shape of the adsorption isotherm curves for all the samples can be considered as a combination of type I and type IV, indicating the presence of microporous and slit shaped pores. The shape of adsorption-desorption isotherm remains the same as those before modification of ZSM-5 implying the modification does not change the pore shapes of the ZSM-5. As can be seen in Table 1, doping ZSM-5 with copper and cerium leads to a slightly decrease in BET surface area and micropore volume, from 380 m^2g^{-1} and 0.14 cm^3g^{-1} respectively for ZSM-5 to 318 m^2g^{-1} and 0.13 cm^3g^{-1} respectively for CuCe4-Z. This can be explained by the fact that copper and cerium species cover the external surface of ZSM-5, blocking a number of zeolite channels, and impeding entry of N_2 into the pores.

XRD patterns of the pure ZSM-5, Cu-Z and CuCe/ZSM-5 catalysts are depicted in Fig. 2. The inherent MFI structure of ZSM-5 was observed (2θ=7.8º，8.7º，24.5º，24.9º，PDF= 44-003) which suggests that the catalysts still maintain the well-ordered microstructure of ZSM-5 after the copper and cerium additions. However, the intensity of the ZSM-5 principal diffraction peaks decreased to a certain extent after the copper and cerium incorporation, probably owing to the higher absorption coefficient of metal compounds for X-ray radiation [26]. No diffraction peaks derived from metal or metal oxide clusters are observed for Cu-Z, CuCe1-Z, CuCe2-Z and

CuCe3-Z, suggesting that the species are well dispersed as amorphous metal species, or aggregated into mini-crystals that are too small to be detected by XRD [27]. With increasing the cerium content to 2.0 wt.%, the peak of CeO_2 are observed for CuCe4-Z (2θ=28.2º， PDF= 34-0394), which is explained by the fact that the extra-framework cerium is prone to agglomerate into cerium oxides clusters.

In order to gain further insight into the distribution of copper and cerium crystallites, the samples are characterized by TEM experiments. A typical bright field TEM image of pure ZSM-5 catalyst is shown in Fig. 3A. The sample is comprised of crystalline ZSM-5 particles, which are dispersed on the amorphous silica-alumina matrix and exhibit characteristic diffraction contrast. It can be seen that a relatively homogeneous distribution of copper particles are obtained over the Cu-Z catalyst (Fig. 3B). The homogeneous distribution observed is agreement with those of XRD. The image in Fig. 3C reveals that the cerium added to the support is preferentially located at the external surface of the ZSM-5 zeolite. The fine particles are relatively spherical in shape and each particle is found to be an aggregate of nano-crystallites.

3.2. XPS analysis

The chemical states and surface proportions of elements for the catalysts were characterized by X-ray photoemission spectroscopy. Fig. 4 shows the XPS spectra of Cu 2p. A low intensity of the shake-up satellite peak in the range of 938-945 eV confirms the existence of Cu^{2+} in the Cu-Z and CuCe-Z catalysts. As a consequence, peak deconvolution and fitting to experimental data show that the experimental Cu

$2p_{3/2}$ peak could be fitted well by having two peaks corresponding to the chemical states Cu^{2+} at 934.3 eV of $2p_{3/2}$ and Cu^{+} at 933.0 eV of $2p_{3/2}$. It can be seem from Fig. 4 that both charge states 1+ and 2+ are present in Cu-Z and CuCe-Z catalysts.

Fig. 5 displays the Ce 3d XPS spectrum of the CuCe4-Z sample. The Ce 3d spectra is complicated and can be individually deconvoluted into $3d_{5/2}$ and $3d_{3/2}$ spin-orbit components (labeled as *v* and *u*, respectively) describing the $Ce^{4+} \leftrightarrow Ce^{3+}$ electronic transitions [28]. The four intense components *v* (BE~882.5 eV), *u* (BE~900.9 eV), *v‴* (BE~898.2 eV), *u‴* (BE~917.1 eV) as well as the two weaker components *v″* (BE~889.4 eV) and *u″* (BE~908.2 eV) can be attributed to Ce^{4+} cations. With respect to the Ce^{3+} cations, the *v′* (BE~885.6 eV) and *u′* (BE~903.7 eV) components are noticeably weaker than those for the Ce^{4+} cations [29-31]. Hence both Ce^{3+} and Ce^{4+} cations coexist in the CuCe-Z catalysts.

Curve-fitting procedures were applied to the O 1s region, as shown in Fig. 6. The O 1s XPS spectrum of Cu-Z shows a strong peak at 531.8 eV, which represents large numbers of lattice oxygen from the ZSM-5 zeolite structure, together with relatively small amounts of chemisorbed oxygen and weakly bonded oxygen species. Field investigations have shown that Ce^{3+} could create a charge imbalance, vacancies and unsaturated chemical bonds on the sample surface, for which more chemisorbed oxygen or/and weakly bonded oxygen species would be brought [32]. These oxygen species play an important role in oxidation reaction [33]. The O 1s XPS spectra of CuCe-Z catalysts show two primary peaks. Similarly to that of the Cu-Z, the peak at a higher binding energy of 531.8 eV may be assigned to regular lattice oxygen from the

ZSM-5 zeolite structure (Oz), chemisorbed oxygen and weakly bonded oxygen species, while the shoulder peak at about 529.7 eV corresponds to lattice oxygen from copper and cerium oxides (Oo).

Table 2 shows that the surface Cu/Si, Ce/Si, Cu^{+}/Cu^{2+}, Ce^{3+}/Ce^{4+} and Oo/Oz atomic ratios over the catalysts. It can be confirmed from the results that the copper and cerium appear to enrich on the surface of ZSM-5 grains, since the Cu/Si and Ce/Si atomic ratios detected by XPS increase monotonously with the cerium content increasing, and are considerably large than those values obtained from AAS. Given that the copper content is set at 2.0 wt.% during the catalyst preparation, the Cu/Si atomic ratios also exhibit an increasing tread with cerium content, indicating that the enriched copper species are perhaps interacting on cerium and are preferentially cover the cerium phases.

The Cu^{+}/Cu^{2+}, Ce^{3+}/Ce^{4+} and Oo/Oz surface atomic ratios calculated according to relative peak areas from XPS spectra are also listed in Table 2. In particular, the concentration of Ce^{3+} and Ce^{4+} cations in CuCe-Z catalysts can be estimated as Eqs. (1) and (2), [34] where the $[Ce^{3+}]$ and $[Ce^{4+}]$ stand for the sums of the integrated peak areas related to their XPS signals respectively:

$$[Ce^{3+}] = v' + u' \qquad (1)$$

$$[Ce^{4+}] = v + v'' + v''' + u + u'' + u''' \qquad (2)$$

As the cerium content increases, the Cu^{+}/Cu^{2+} and Ce^{3+}/Ce^{4+} ratios are reduced from 1.142 (Cu-Z) to 0.816 (CuCe4-Z) and from 0.279 (CuCe1-Z) to 0.232 (CuCe4-Z), respectively. Moreover, the Oo/Oz surface atomic ratio exhibits an increasing trend

with cerium content. Combined with the XRD results, the overfull cerium enriched on the ZSM-5 support is easily aggregated and sintered to formed bulk CeO_2 during the calcination process. As such, the decrease of Ce^{3+}/Ce^{4+} ratio is probably caused by the formation of the ceria. Concerning the Cu 2p spectra, most copper initially present in these samples is in a +2 oxidation state and small amount in a +1 oxidation state for the CuCe-Z catalysts, located at 934.3 and 933.0 eV, respectively. The copper and cerium interaction acts as a reservoir of finely dispersed copper species ensuring high catalytic activity [35]. We propose that part of copper ions have probably entered the ceria lattice, which lead to form low concentration of Ce^{3+} defects.

3.3. Temperature-programmed desorption of ammonia

Fig. 7 shows the NH_3-TPD results obtained for pure ZSM-5, Cu-Z and CuCe-Z samples. In the case of the parent H-ZSM-5, three NH_3 desorption peaks at maximum temperatures of about 110, 170 and 320 °C are clearly observed. Here, the peaks located at 110 and 170 °C can be reasonably ascribed to weak acidic sites, arising from NH_3 physisorbed on Si–OH or from non-zeolitic impurities. The peak located at 320 °C can be ascribed to the strong acidic sites, assigned to NH_3 bound to strong acid sites. Upon introduction of copper and cerium, the maximum temperatures of α and β peaks are slightly increased, indicative of a slight increase in the intensity of the weak acidic sites, whereas the γ peaks decrease considerably. The nitrogen sorption results (Fig. 1 and Table 1) have confirmed that the increase of the cerium loading leads to the blockage of partial micropores and decrease of BET surface area. Thus, the γ

desorption peak vanishes when the copper is introduced, indicating that some copper ions are exchanged on the acid sites or partial copper species enriched on the ZSM-5 surface covers acid sites. With the cerium content increasing, some new NH_3 desorption peaks appear at the high temperature > 250 °C for the CuCe-Z samples, indicating the formation of stronger acid sites. It is reasonable to conclude that the ammonia chemisorption at temperatures higher than 250 °C is mainly due to cerium oxide nanoclusters. Combined with the finding from TEM and XPS that the cerium is enriched on the surface of ZSM-5 grains, there should be a correlation between the quantity of chemisorbed ammonia and number of cerium ions exposed on the surface of the active phase. Likely, ammonia molecules are bonded to cerium by donor–acceptor bond, which is formed by attaching the free electron pair of ammonia into unoccupied d-orbitals of cerium.

3.4. Temperature-programmed reduction of hydrogen

Temperature-programmed reduction experiments were carried out to get further insights into copper species and their redox properties. The obtained profiles are shown in Fig. 8 and the results are listed in Table 3. The nature of the copper species present in the ZSM-5 zeolite is commonly discussed on basis of the position of the H_2 consumption peaks and the peak areas. For the pure ZSM-5 sample, there is no obvious reduction peak during the H_2 reduction process. TPR profile of the Cu-Z sample exhibits two reduction peaks at 227 and 280 °C, respectively. The α peak at 227 °C is attributed to the reduction of copper species dispersed on the ZSM-5

support, while the β peak at 280 °C corresponds to the reduction of the copper oxides adhering to the external surface of ZSM-5 crystallites. These oxides aggregate to form crystallites that are too small to be detected by XRD. Upon addition of cerium, TPR curves of CuCe-Z samples exhibit four reduction peaks at about 200, 230, 270 and 380 °C. Similar to the Cu-Z sample, the α (222 °C) and β (276 °C) peaks of CuCe-Z samples are assigned to the dispersed copper clusters and copper oxides, respectively. As shown in Table 3, the H_2 consumption for the α peaks are in the range of 25-27μmol H_2 g^{-1} with the cerium content increasing from 0 (Cu-Z) to 1.0 wt.% (CuCe2-Z). Significant increase of H_2 consumption for the α peaks can be found when the cerium content is higher than 1.0 wt.%, reaching 57 μmol H_2 g^{-1} for CuCe3-Z and 64 μmol H_2 g^{-1} for CuCe4-Z, respectively. By contrast, the H_2 consumption for the β peaks decreases. These results indicate that the cerium introduction promotes the dispersion of copper species. Combined with the XPS results, it is reasonable to deduce that these copper species in proximity to the cerium phase are reduced more easily by hydrogen than those on the pure ZSM-5 support. After the cerium addition, the γ and δ peaks appear for the CuCe-Z samples. Possibly, some copper ions are incorporated into the vacant sites of the cerium oxides to form an oxygen-capped surface structure, although the solubility of copper into the ceria network is low. The formation of mixed oxides results in coordinative unsaturated species and thus increases oxygen mobility. Hence reduction is no longer confined to the surface of the material, but extends deep into its bulk, which may accelerate the reduction process and consume more hydrogen. Compared to the Cu-Z sample loaded

mono-metal, the samples modified by cerium-metal consumed more hydrogen during the reduction process (as shown in Table 3) and obtain the maximum of 202 μmol H_2 g^{-1} for the CuCe3-Z, which testify that more reduction species have been obtained for the CuCe-Z samples than that of the Cu-Z.

3.5. Catalytic activity tests

Fig. 9 shows the NO conversion in the SCR reaction on the pure ZSM-5, Cu-Z and CuCe-Z catalysts from 50 to 300 ºC. Pure ZSM-5 is inactive over the entire temperature range studied. The Cu-Z and CuCe-Z catalysts exhibit a similar trend of NO conversions, and more importantly the CuCe-Z catalysts characterized by higher cerium content exhibit better catalytic performances. On the one hand, the cerium introduction into Cu-Z enhances their low-temperature activities. The light-off temperature (10% NO conversion) is reached at 103 ºC for Cu-Z while the value is shifted to 60 ºC when the cerium content increases in CuCe4-Z. 95% NO conversion is reached around 197 ºC for Cu-Z while the corresponding temperature value decreases to 148 ºC for CuCe4-Z. All the samples reach the full conversion above 205 ºC. On the other hand, when the cerium are added to Cu/ZSM-5, the temperature range of efficient NO reduction (95%) also extends to higher temperature. Among the Cu-Ce/ZSM-5 catalysts tested, the CuCe4-Z sample exhibits the highest catalytic activity with the temperature range for 90% NO removal of 148-427 ºC. The SCR process induced by all the catalysts produces N_2O and NO_2 as byproducts. In the whole range of this study, however, it can be observed that N_2O and NO_2

concentrations are below 10 ppm on all the catalysts. In this case, the NO selectivity to N_2 is close to 100%.

It is widely accepted that in a typical heterogeneous catalytic reaction, the adsorption of reactants and the activation of adsorbed species are both required for the process to occur. the SCR process on Cu-Z and CuCe-Z catalysts involves three sequential reactions in the catalytic cycle [36]: (i) Cu^+ species are preferentially oxidized by O_2 to form Cu^{2+} species; (ii) the oxygen in the atmosphere then reacts with NO to produce a surface nitrogen oxide intermediate bound to Cu^{2+} , namely "Cu^{2+}-N_xO_y"; (iii) the resulting Cu^{2+}-N_xO_y active intermediate reacts with ammonia to yield N_2 and H_2O, accompanied by the regeneration of Cu^+. The Cu-Z catalyst with outstanding activity is a good candidate for the selective catalytic reduction of NO by NH_3. As expected, the introduction of cerium significant promotes the activity of Cu-Z, and the activity of catalyst increases with the increase of cerium content. According to the XRD results, the cerium addition has little influence on copper dispersion. A good dispersion of copper species, giving an intimate contact with the ZSM-5 support, leads to a stronger tendency for copper to be oxidized and thus stabilizes copper species against decomposition or reduction. The highly dispersed copper species are enriched on the surface of ZSM-5 grains. According to the TEM results, a fraction of the copper and cerium oxide clusters are probably located on the outer surfaces of ZSM-5 crystals. The XPS analysis also confirms that the ratios of Cu/Si and Ce/Si are higher than that from AAS results. The enrichment of copper species inclined to highly disperse on the catalyst surface provide better contact

conditions for the NO conversion. The appropriate cerium addition enhances redox ability. According to the literature [37], the facile Ce^{4+}/Ce^{3+} redox cycle can promote the transformation of Cu^{+} to Cu^{2+} involving the following step: $Cu^{2+}+Ce^{3+}\leftrightarrow Cu^{+}+Ce^{4+}$, and hence resulting in a higher content of Cu^{2+} species in the cerium-containing catalysts. Due to the existence of Ce^{3+}/Ce^{4+} redox couple in cerium-containing catalysts, the coordinative unsaturates formed in the mixed oxides lead to the reduction no longer confined to the surface, but extended deep into the bulk of the material, which may accelerate the reduction process.

4. Conclusion

The present study focused on the effects of ceria addition on the structures and copper species in copper based ZSM-5 catalysts. The catalytic behavior of obtained catalysts was tested in selective catalytic reduction of NO_x using ammonia as reductant. It was found that the addition of cerium increased copper dispersion and prevented its crystallization. Copper species were enriched on the ZSM-5 grain surfaces and part of copper ions was incorporated into the cerium lattice. Moreover, Addition of cerium improved the redox properties of the CuCe/ZSM-5 catalysts, which arose from the higher valence of copper and mobility of lattice oxygen than those of Cu/ZSM-5 catalyst, which have been confirmed in the XPS and H_2-TPR analysis. In this case, when the cerium are introduced into the Cu/ZSM-5, the temperature range of efficient NO reduction (95%) extends to both lower and higher temperatures, i.e. the active window widens. Among the CuCe/ZSM-5 catalysts tested, the CuCe4-Z exhibits the highest catalytic activity with the temperature range of 95%

NO removal of 148-427 ºC.

Acknowlegements

This study was supported by the National Natural Science Foundation of China (21307088) and the Tianjin Research Program of Application Foundation and Advanced Technology (10JCZDJC24900).

References

[1] H. Chang, L. Ma, S. Yang, J. Li, L. Chen, W. Wang, J. Hao, Comparison of preparation methods for ceria catalyst and the effect of surface and bulk sulfates on its activity toward NH_3-SCR, J. Hazard. Mater. 262 (2013) 782– 788.

[2] M. Iwamoto, H. Yahiro, Y. Mine, S. Kagawa, Excessively copper ion-exchanged ZSM-5 zeolites as highly active catalysts for direct decomposition of nitrogen monoxide, Chem. Lett. 18 (1989) 213–216.

[3] L. Olsson, H. Sjövall, R.J. Blint, A kinetic model for ammonia selective catalytic reduction over Cu-ZSM-5, Appl. Catal. B 81 (2008) 203–217.

[4] X.F. Yang , Z.l. Wu, M. Moses-Debusk , D.R. Mullins, S.M. Mahurin, R. A. Geiger, M. Kidder, C. K. Narula, Heterometal incorporation in metal-exchanged zeolites enables low-temperature catalytic activity of NO_x reduction, J. Phys. Chem. C 116 (2012) 23322–23331.

[5] B. Greenhalgh, M. Fee, J. Moir, R. Burich, J.P. Charland, M. Stanciulescu, DeNOx activity-TPD correlations of NH_3-SCR catalysts, J. Mol. Catal. A

333(2010) 121–127.

[6] Z. Chajar, M. Primet, H. Praliaud, M. Chevrier, C. Gauthier, F. Mathis, Nitrogen dioxide effect in the reduction of nitric oxide by propane in oxidizing atmosphere, Chem. Lett. 28 (1994) 33–40.

[7] M. Occhiuzzi, G. Fierro, G. Ferraris, G. Moretti, Unusual complete reduction of Cu^{2+} species in Cu-ZSM-5 zeolites under vacuum treatment at high temperature, Chem. Mater. 24 (2012) 2022–2031.

[8] J.H. Kwak, D. Tran, S. D. Burton, J. Szanyi, J.H. Lee, C.H.F. Peden, Effects of hydrothermal aging on NH_3-SCR reaction over Cu/zeolites, J. Catal. 287(2012) 203–209.

[9] C. Torre-Abreu, M.F. Ribeiro, C. Henriques, G. Delahay, Characterisation of CuMFI catalysts by temperature programmed desorption of NO and temperature programmed reduction: Effect of the zeolite Si/Al ratio and copper loading, Appl. Catal. B 12(1997) 249–262.

[10] R. Nedyalkova, C. Montreuil, C. Lambert, L. Olsson, Inter zeolite conversion of FAU type zeolite into CHA and its application in NH_3-SCR, Top. Catal. 56 (2013) 550–557.

[11] G. Moretti, C. Dossi, A. Fusi, S. Recchia, R. Psaro, A comparison between Cu-ZSM-5, Cu-S-1 and Cu-mesoporous-silica-alumina as catalysts for NO decomposition, Appl. Catal. B 20(1999) 67–73.

[12] S. Dzwigaj, J. Janas, J. Gurgul, R.P. Socha, T. Shishido, M. Che, Do Cu(II) ions need Al atoms in their environment to make CuSiBEA active in the SCR of NO

by ethanol or propane? A spectroscopy and catalysis study, Appl. Catal. B 85 (2009) 131–138.

[13] A. Boix, E.E. Mir, E.A. Lombardo, M.A. M.A. Bañares, R. Mariscal, J.L.G. Fierro, The nature of cobalt species in Co and $PtCoZSM_5$ used for the SCR of NO_x with CH_4, J. Catal. 217 (2003) 186–194.

[14] M.C. Campa, S. De Rossi, G. Ferraris, V. Indovina, Catalytic activity of Co-ZSM-5 for the abatement of NO_x with methane in the presence of oxygen, Appl. Catal. B 8 (1996) 315–331.

[15] F. Liu, H. He, Y. Ding, C. Zhang, Effect of manganese substitution on the structure and activity of iron titanate catalyst for the selective catalytic reduction of NO with NH_3, Appl. Catal. B 93 (2009) 194–204.

[16] G. Picasso, M. Gutierrez, M.P. Pina, J. Herguido, Preparation and characterization of Ce-Zr and Ce-Mn based oxides for n-hexane combustion: Application to catalytic membrane reactors, Chem. Eng. J. 126 (2007) 119–130.

[17] L. Katta, P. Sudarsanam, G. Thrimurthulu, B.M. Reddy. Doped nanosized ceria solid solutions for low temperature soot oxidation: Zirconium versus lanthanum promoters, Appl. Catal. B 101 (2010) 101–108.

[18] O.H. Laguna, F. Romero Sarria, M.A. Centeno, J.A. Odriozola. Gold supported on metal-doped ceria catalysts (M = Zr, Zn and Fe) for the preferential oxidation of CO (PROX), J. Catal. 276(2010) 360–370.

[19] T. Sowade, T. Liese, C. Schmidt, F.W. Schutze, X. Yu, H. Berndt, W. Grunert, Relations between structure and catalytic activity of Ce-In-ZSM-5 catalysts for

the selective reduction of NO by methane: II. Interplay between the CeO_2 promoter and different indium sites, J. Catal. 225(2004) 105–115.

[20] G. Qi, R.T. Yang, R. Chang, MnO_x-CeO_2 mixed oxides prepared by co-precipitation for selective catalytic reduction of NO with NH_3 at low temperatures, Appl. Catal. B 51(2004) 93–106.

[21] G. Carja, Y. Kameshima, K. Okada, C.D. Madhusoodana, Mn-Ce/ZSM_5 as a new superior catalyst for NO reduction with NH_3. Appl. Catal. B 73 (2007) 60–64.

[22] X. Wu, Q. Liang, D. Weng, Z. Lu, The catalytic activity of CuO–CeO_2 mixed oxides for diesel soot oxidation with a NO/O_2 mixture, Catal. Commun. 8 (2007) 2110–2114.

[23] R. Dziembaj, M. Molenda, M.M. Zaitz, L. Chmielarz, K. Furczoń, Correlation of electrical properties of nanometric copper-doped ceria materials ($Ce_{1-x}Cu_xO_{2-\delta}$) with their catalytic activity in incineration of VOCs, Solid State Ionics 251 (2013) 18–22.

[24] N.C. Pérez, E.E. Miró, J.M. Zamaro, Cu,Ce/mordenite coatings on FeCrAl- alloy corrugated foils employed as catalytic microreactors for CO oxidation, Catal. Today 213 (2013) 183–191.

[25] P. Praserthdam, C. Chaisuk, A. Panit, K. Kraiwattanawong, Some aspects about the nature of surface species on Pt-based and MFI-based catalysts for the selective catalytic reduction of NO by propene under lean-burn condition, Appl. Catal. B 38 (2002) 227–241.

[26] G. Qi, R.T. Yang, Selective catalytic oxidation (SCO) of ammonia to nitrogen

over Fe/ZSM-5 catalysts, Appl. Catal. A 287 (2005) 25–33.

[27] H. Ohtsuka, T. Tabata, O. Okada, L.M. Sabatino, G. Bellussi, A study on selective reduction of NO_x by propane on Co-Beta, Catal. Let. 44 (1997) 265–270.

[28] F. Zhang, P. Wang, J. Koberstein, S. Khalid, S.W. Chan, Cerium oxidation state in ceria nanoparticles studied with X-ray photoelectron spectroscopy and absorption near edge spectroscopy, Surf. Sci. 563 (2004) 74–82.

[29] S. Damyanova, B. Pawelec, K. Arishtirova, M. V. Martinez Huerta, J. L. G. Fierro, Study of the surface and redox properties of ceria–zirconia oxides, Appl. Catal. A: Gen. 337 (2008) 86–96.

[30] J. Guo, D. Wu, L. Zhang, M. Gong, M. Zhao, Y. Chen. J. Preparation of nanometric CeO_2-ZrO_2-Nd_2O_3 solid solution and its catalytic performances, Alloys Compd. 460 (2008) 485–490.

[31] J. Fan, X. Wu, L. Yang, D. Weng, The SMSI between supported platinum and CeO_2-ZrO_2-La_2O_3 mixed oxides in oxidative atmosphere, Catal. Today 126 (2007) 303–312.

[32] Q. Wan, L. Duan, K. He, J. Li, Removal of gaseous elemental mercury over aCeO_2–WO_3/TiO_2 nanocomposite in simulated coal-fired flue gas, Chem. Eng. J. 170 (2011) 512–517.

[33] H. Li, C. Y. Wu, Y. Li, J. Zhang, CeO_2-TiO_2 catalysts for catalytic oxidation of elemental mercury in low-rank coal combustion flue gas, Environ. Sci. Technol. 45 (2011) 7394–7400.

[34] E.Y. Konysheva, S.M. Francis, Identification of surface composition and

chemical states in composites comprised of phases with fluorite and perovskite structures by X-ray photoelectron spectroscopy, Appl. Surf. Sci. 268(2013) 278–287.

[35] R. Si, J. Raitano, N. Yia, L. Zhang, S.-W. Chan, M. Flytzani-Stephanopoulos, Structure sensitivity of the low-temperature water-gas shift reaction on Cu-CeO_2 catalysts, Catal. Today 180 (2012) 68–80.

[36] G. Delahay, S. Kieger, N. Tanchoux, P. Trens, B. Coq, Kinetics of the selective catalytic reduction of NO by NH_3 on a Cu-faujasite catalyst, Appl. Catal. B 52 (2004) 251–257.

[37] A. Aboukais, A. Bennani, C. Lamonier-Dulongpont, E. Abi-Aad, G. Wrobel, Redox behaviour of copper (II) species on CuCe oxide catalysts: electron paramagnetic resonance (EPR) study, Colloids Surf. A 115 (1996) 171–177.

Table 1. Physico-chemical properties of pure ZSM-5, Cu-Z and CuCe-Z catalysts.

Sample	BET surface area (m^2g^{-1})	Average pore diameter (nm)	Micro-pore volume (cm^3g^{-1})
ZSM-5	380	2.0	0.14
Cu-Z	354	1.9	0.13
CuCe1-Z	347	1.9	0.13
CuCe2-Z	342	1.9	0.13
CuCe3-Z	337	1.9	0.13
CuCe4-Z	318	1.9	0.13

Table 2. Surface composition of Cu-Z and CuCe-Z catalysts derived from XPS analysis.

Sample	Cu/Si		Ce/Si		Cu^{+}/Cu^{2+}	Ce^{3+}/Ce^{4+}	Oo/Oz
	AAS	XPS	AAS	XPS			
Cu-Z	0.011	0.039	0	0	1.142	/	0
CuCe1-Z	0.011	0.047	0.002	0.008	0.996	0.279	0.029
CuCe2-Z	0.011	0.049	0.004	0.011	0.961	0.252	0.087
CuCe3-Z	0.011	0.058	0.006	0.024	0.867	0.246	0.178
CuCe4-Z	0.011	0.065	0.008	0.029	0.816	0.232	0.392

Table 3. Results of hydrogen consumption of pure ZSM-5, Cu-Z and CuCe-Z catalysts.

Sample	Γ		α		β		δ		Total H_2 consumption (μmol H_2g^{-1})
	Center (°C)	H_2 consumption (μmol H_2g^{-1})	Center (°C)	H_2 consumption (μmol H_2g^{-1})	Center (°C)	H_2 consumption (μmol H_2g^{-1})	Center (°C)	H_2 consumption (μmol H_2g^{-1})	
Pure ZSM-5	-	-	-	-	-	-	-	-	-
Cu-Z	-	-	227	27	280	121		-	148
CuCe1-Z	205	16	239	25	277	87	402	49	177
CuCe2-Z	187	12	220	25	269	79	393	26	142
CuCe3-Z	201	22	232	57	273	61	370	62	202
CuCe4-Z	198	36	232	64	270	42	368	22	164

Figure Captions

Fig. 1. Nitrogen adsorption/desorption isotherms of pure ZSM-5, Cu-Z and CuCe-Z catalysts: (a) pure ZSM-5; (b) Cu-Z; (c) CuCe1-Z; (d) CuCe2-Z; (e) CuCe3-Z; (f) CuCe4-Z.

Fig. 2. XRD patterns of pure ZSM-5, Cu-Z-5 and CuCe-Z catalysts: (a) pure ZSM-5; (b) Cu-Z; (c) CuCe1-Z; (d) CuCe2-Z; (e) CuCe3-Z; (f) CuCe4-Z.

Fig. 3. TEM images of pure ZSM-5 (A), Cu-Z (B) and CuCe4-Z (C) samples.

Fig. 4. Typical XPS narrow spectra Cu 2p from Cu-Z (a) and CuCe4-Z (b) catalysts.

Fig. 5. Typical XPS narrow spectra Ce 3d from CuCe4-Z catalysts.

Fig. 6. Typical XPS narrow spectra O 1s from Cu-Z (a) and CuCe4-Z (b) catalysts.

Fig. 7. NH_3-TPD curves of pure ZSM-5 (a), Cu-Z (b), CuCe1-Z (c), CuCe2-Z (d), CuCe3-Z (e) and CuZr-Z (f) catalysts.

Fig. 8. H_2-TPR curves of pure ZSM-5 (a), Cu-Z (b), CuCe1-Z (c), CuCe2-Z (d), CuCe3-Z (e) and CuZr-Z (f) catalysts.

Fig. 9. Catalytic activities for NO reduction by NH_3 for pure ZSM-5, Cu-Z, CuCe1-Z, CuCe2-Z, CuCe3-Z and CuZr-Z catalysts.

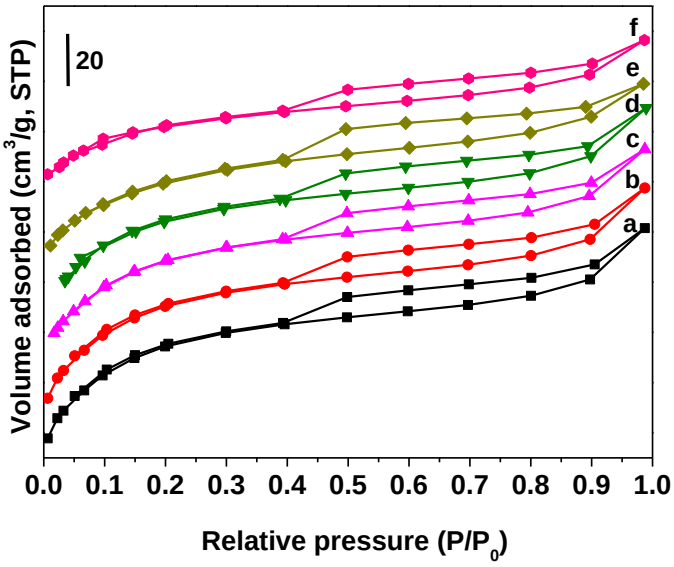
20
f
e
d
c
b
a
Volume adsorbed (cm3/g, STP)
0.0
0.1
0.2
0.3
0.4
0.5
0.6
0.7
0.8
0.9
1.0
Relative pressure (P/P0)

Fig. 1.

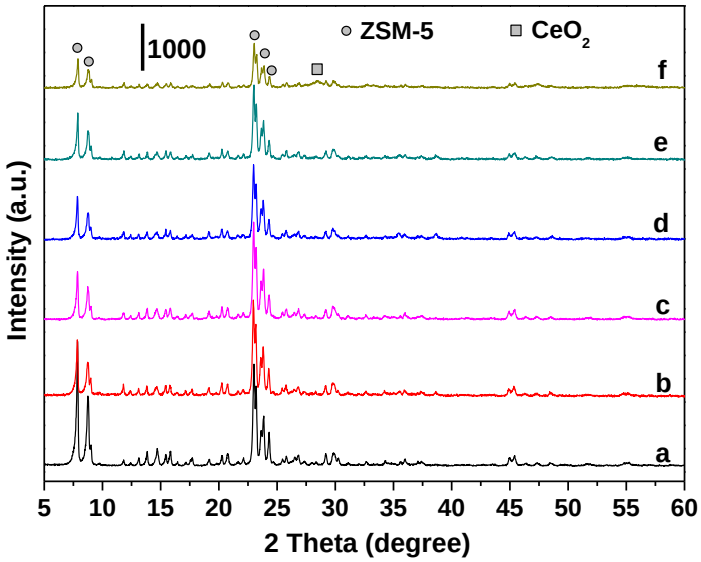
1000
ZSM-5
CeO2
f
e
d
c
b
a
Intensity (a.u.)
5
10
15
20
25
30
35
40
45
50
55
60
2 Theta (degree)

Fig. 2.

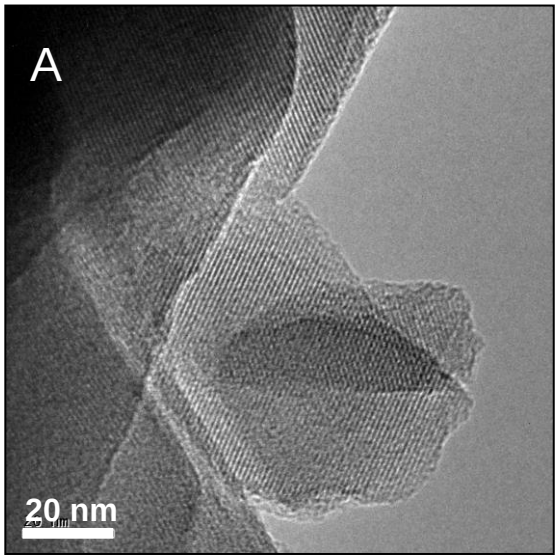
A
20 nm

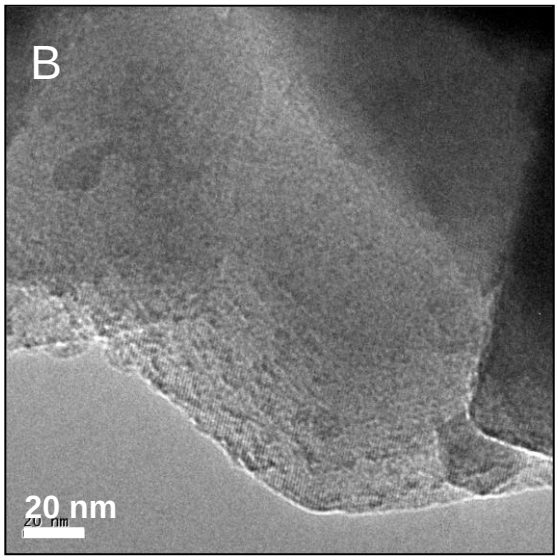
B
20 nm

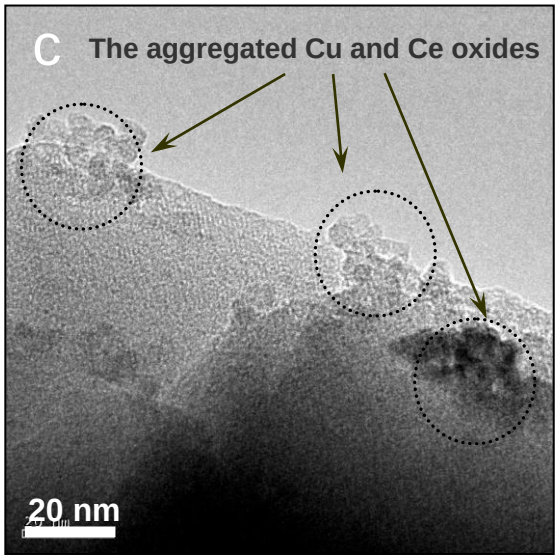
C
The aggregated Cu and Ce oxides
20 nm

Fig. 3.

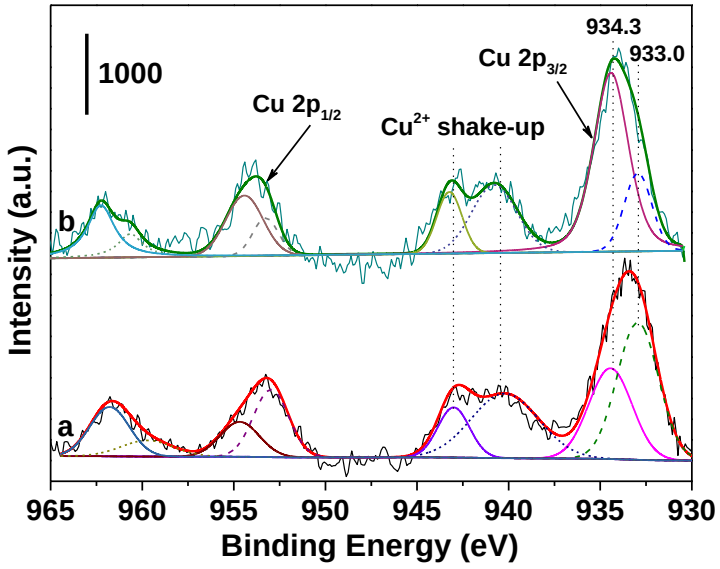
1000
Cu 2p1/2
Cu2+ shake-up
Cu 2p3/2
934.3
933.0
b
a
Intensity (a.u.)
965
960
955
950
945
940
935
930
Binding Energy (eV)

Fig. 4.

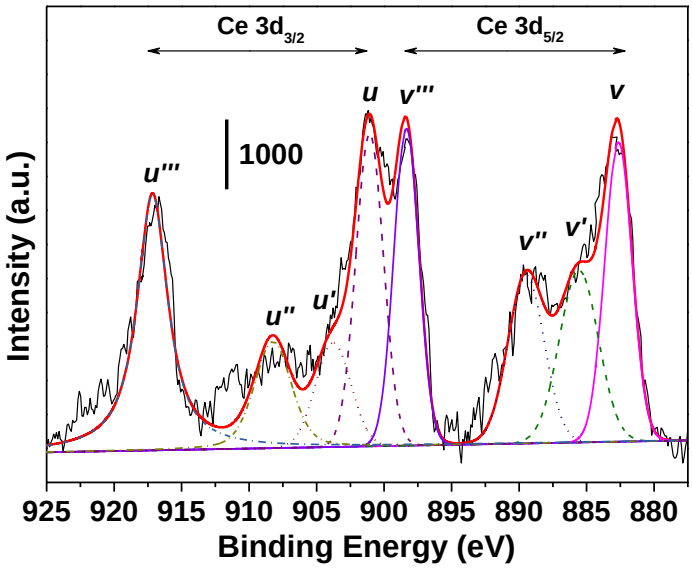
Ce 3d3/2
Ce 3d5/2
u
v'''
v
1000
u'''
u''
u'
v''
v'
Intensity (a.u.)
925 920 915 910 905 900 895 890 885 880
Binding Energy (eV)

Fig. 5.

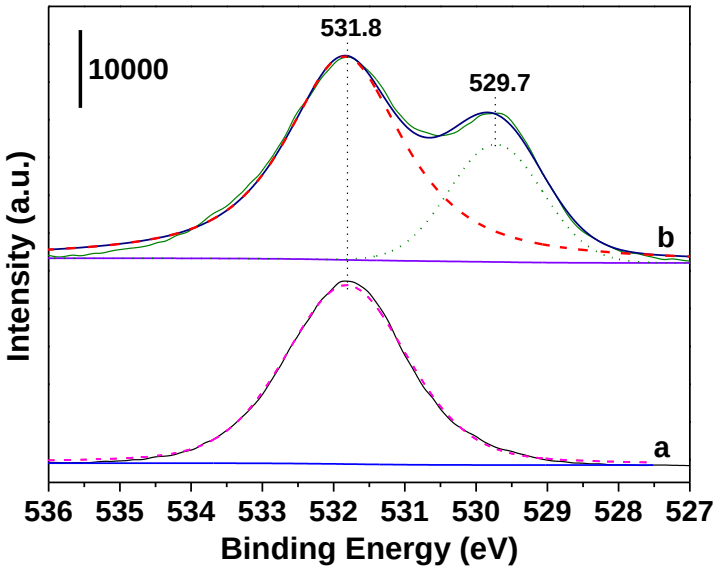
531.8
529.7
10000
b
a
Intensity (a.u.)
536 535 534 533 532 531 530 529 528 527
Binding Energy (eV)

Fig. 6.

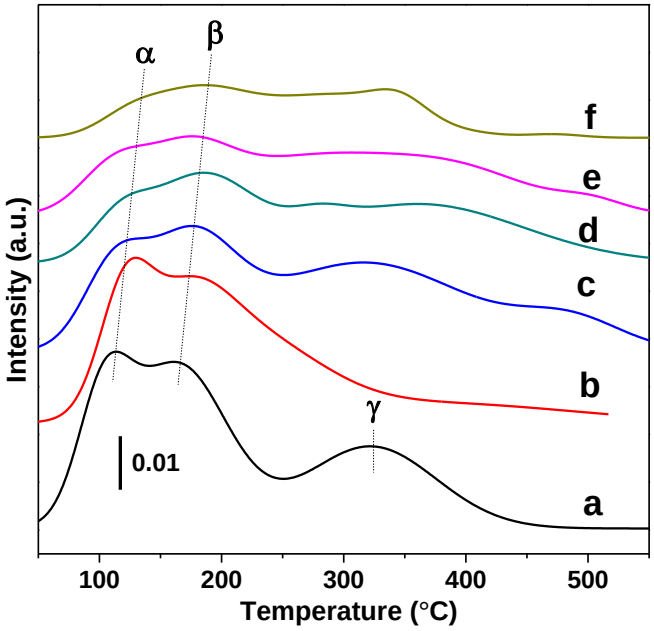
α
β
γ
f
e
d
c
b
a
0.01
Intensity (a.u.)
100
200
300
400
500
Temperature (°C)

Fig. 7.

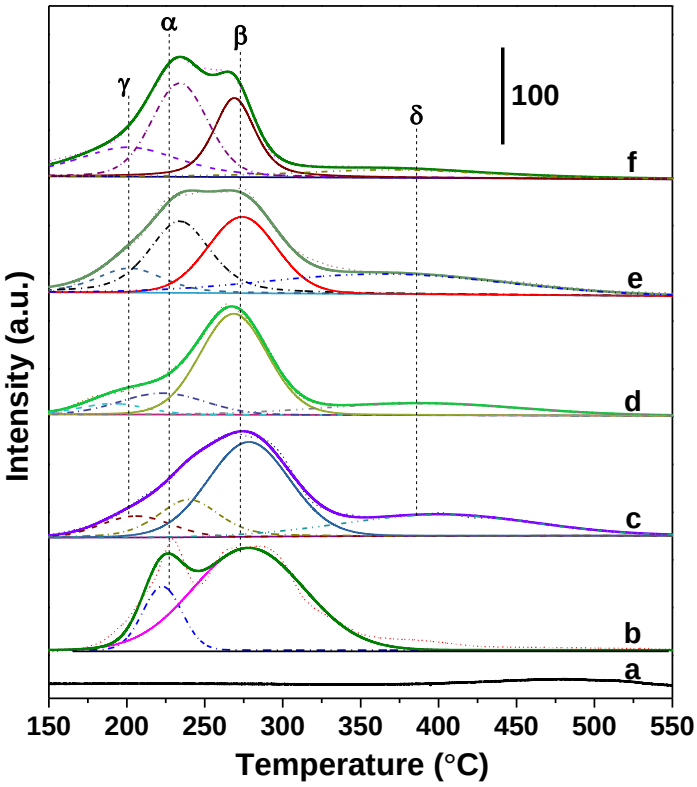
α
β
γ
δ
100
f
e
d
c
b
a
Intensity (a.u.)
150
200
250
300
350
400
450
500
550
Temperature (°C)

Fig. 8.

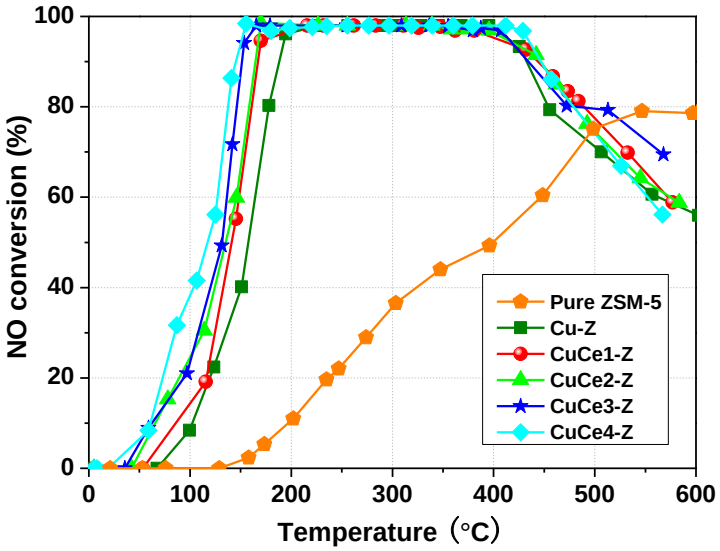
NO conversion (%)
Temperature（°C）
0
20
40
60
80
100
0
100
200
300
400
500
600
Pure ZSM-5
Cu-Z
CuCe1-Z
CuCe2-Z
CuCe3-Z
CuCe4-Z

Fig. 9.